Supporting Information

Adsorption of U(VI) on Stoichiometric and Oxidised Mackinawite; a DFT Study

Naomi E. R. Ofili[1], Adam Thetford[1], Nikolas Kaltsoyannis[1*]

[1]Department of Chemistry, The University of Manchester, Oxford Road, Manchester, M13 9PL, UK

This document contains 12 pages, 5 figures and 4 tables.

Contents

1 Further computational and model details

Periodic boundary conditions and Projector Augmented Wave (PAW) pseudopotentials, which include relativistic effects, were used.[1,2] A plane wave cut-off energy of 600 eV was used and the *k* point sampling was conducted using the Monkhorst-Pack (MP) algorithm.[3] A MP grid of 3×3×1 was used for slab calculations and only the Γ-point was used for molecular calculations. The PBE functional was used to treat exchange and correlation[4,5] along with a U_{eff} potential of 4.0 eV applied to the uranium *f* orbitals to counter the artificial stabilisation of delocalised states for highly correlated electrons in pure DFT. The PBE+*U* method is widely used in the study of highly correlated systems such as those in the 3d and 5f series, including our own work on water adsorption on actinide dioxide surfaces, in which it has been found to produce reliable adsorption energies.[6–8] Previous studies, and our calculations, indicate that mackinawite is a metallic material and so a U_{eff} potential is not required for the Fe *d*-electrons.[9–11] The electrons treated as valence for each element were as follows: H, $1s^1$; O, $2s^2 2p^4$; S, $3s^2 3p^4$; Fe, $3d^7 4s^1$; U, $5f^2 6s^2 6p^6 6d^2 7s^2$. Dispersion forces were modelled using the D3 method.[12] VASPsol, a self-consistent continuum solvation model, was used for the implicit solvation calculations to simulate a neutral aqueous environment.[13,14] A relative permittivity of 78.4 which is the value for water at 298 K and 1 MPa was applied.[15] Calculations were considered converged when the residual atomic forces were <0.02 eV $Å^{-1}$ and a tolerance of 10^{-4} eV was applied for the electronic minimisations.

Mackinawite has a layered structure formed of sheets of edge-sharing FeS_4 tetrahedra. An antiferromagnetic single-stripe magnetic ordering, calculated by Kwon *et al*. and ourselves to be the ground state magnetic ordering of mackinawite, was used.[9] The optimised lattice parameters ($a = b$ = 3.584 Å, c = 5.028 Å) matched well with the experimental values ($a = b$ = 3.6735 Å, c = 5.0328 Å).[16] The slab was built with three FeS layers and a 15 Å vacuum gap was used avoid interactions with the periodic images in the *z* direction.

The uranyl complex is large at ~5 Å in diameter and long-range dispersion forces were included in the calculations. To avoid interaction between the periodic images of the complex in the *x* and *y* directions, the slab was constructed with 16 unit cells per layer (4×4) which produces a surface area of

14.34 Å^2. This gives ~10 Å between the repeated images of the complex. During the adsorption calculations, atom positions in the top two layers were allowed to relax whereas atoms in the bottom layer were fixed in the bulk equilibrium positions. The box size remained fixed at 14.34 × 14.34 × 29.00 Å for all slab and adsorption calculations.

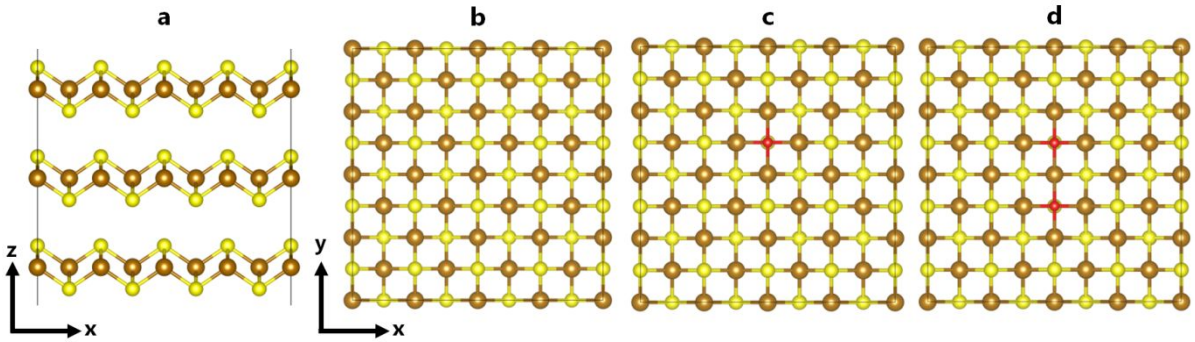

Figure S1. Stoichiometric and oxidised mackinawite slabs: a and b = FeS; c = FeS-1O; d = FeS-2O. Brown = Fe; yellow = S; red = O.

2 FeS

2.1 Models 1-3 results

Table S1. Adsorption energies, E_{ads}, shortest U-S distances and the difference between the U *z* coordinate and the average *z* coordinate of the closest S atoms for each adsorption mode in each model.

Adsorption mode	Model	E_{ads} / kJ mol^{-1}	U-S / Å	U(*z*)-S(*z*) / Å
OS-para-S	1 and 2	-49	5.24, 5.33	5.10
	3	-30	5.28, 5.33	4.98
OS-para-h	1 and 2	-55	5.43, 5.44, 5.46, 5.47	5.21
	3	-31	5.69, 5.69, 5.77, 5.77	5.13
OS-perp-h	1 and 2	-67	4.39, 4.40, 4.56, 4.57	3.82
	3	-52	4.44, 4.47, 4.62, 4.65	3.75
OS-perp-S	1 and 2	-80	4.21, 5.34, 5.38	4.29
	3	-66	4.13, 5.42, 5.44	4.07
OS-perp-Fe	1 and 2	-87	4.32, 4.47	4.06
	3	-69	4.32, 4.43	3.96
IS-mono-5	1	-54	3.05	3.06
	2	-111	3.11	3.19
	3	-65	3.30	3.26
IS-mono-4	1	-6	2.95	3.01
	2	-114	2.96	2.98
	3	-51	2.96	2.90
IS-bid	1	-8	3.13, 3.30	2.72
	2	-101	3.18, 3.21	2.70
	3	-42	3.19, 3.16	2.60
IS-multi	1	16	4.21, 4.25, 4.29, 4.34	3.55
	2	-97	3.66, 3.84, 3.94, 4.11	2.84
	3	-37	3.21, 3.22, 4.44, 4.45	2.59

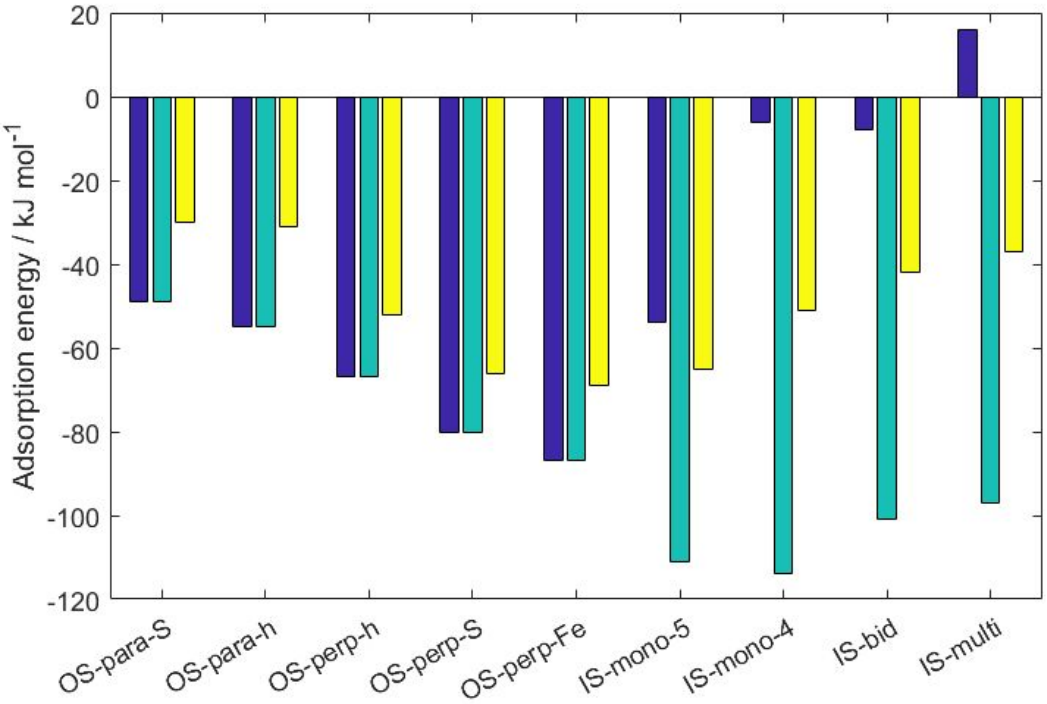

Figure S2. Adsorption energies of each adsorption mode on FeS: purple = Model 1 (displaced H_2O on surface), blue = Model 2 (displaced H_2O in the second coordination sphere), yellow = Model 3 (displaced H_2O in the second coordination sphere with use of an implicit solvation model for water).

2.2 Model 3 U(VI) complex solvation and charge analysis

The solvation energy, ΔE_{sol}, the U(VI) complex was calculated *via* Equation 1 from the main paper. The complex was found to have a negative solvation energy of -130 kJ mol^{-1} indicating that it is more stable in aqueous solution than in vacuum.

Table S2. Bader charge analysis of U in the isolated U(VI) complex and the surface complexes on FeS with the implicit solvation model (Model 3).

System	Bader charge of U / e
U(VI) complex	2.97
OS-para-S	2.98
OS-para-h	2.97
OS-perp-h	3.01
OS-perp-S	2.97
OS-perp-Fe	2.99
IS-mono-5	2.89
IS-mono-4	2.89
IS-bid	2.85
IS-multi	2.89

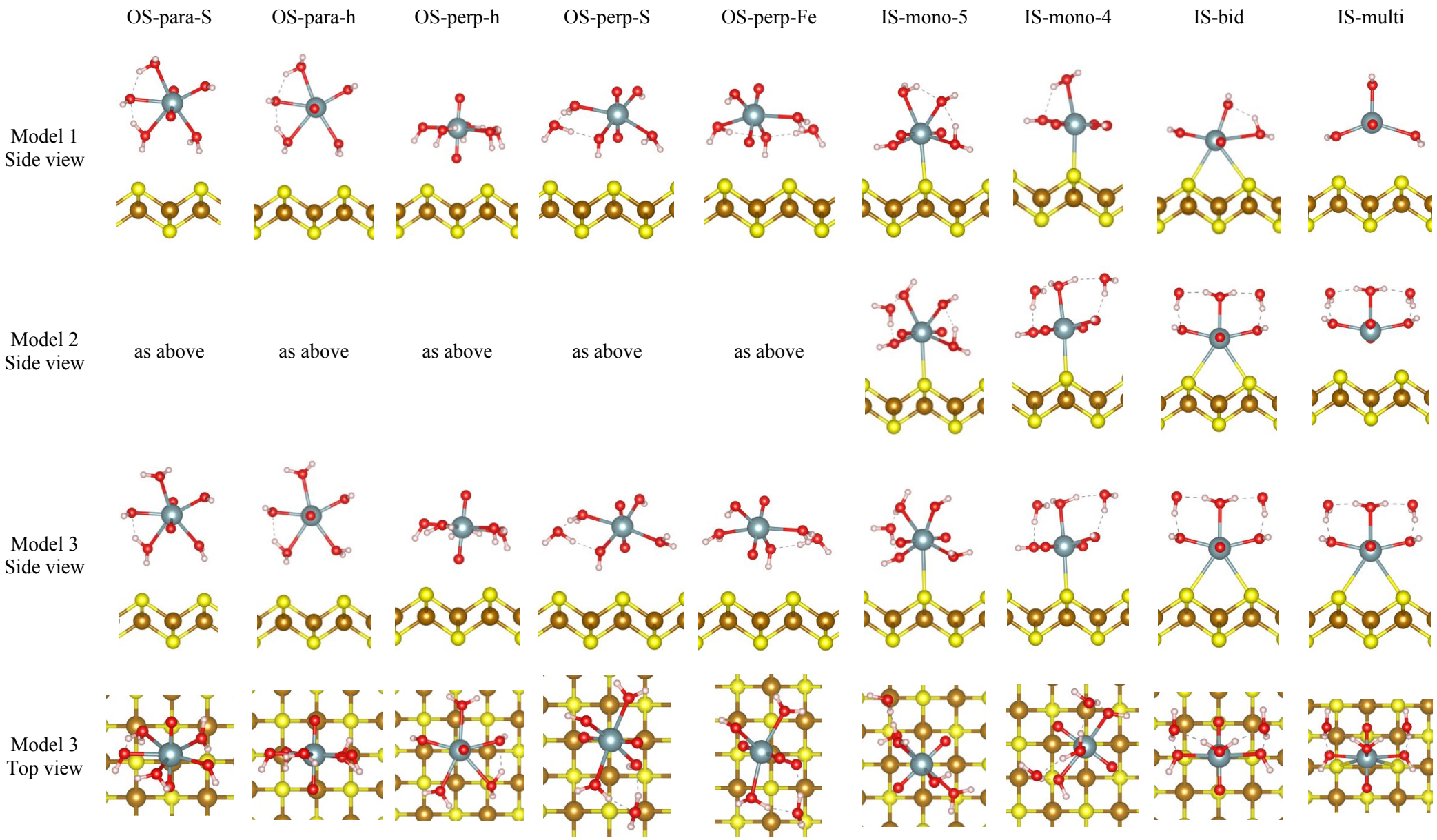

Figure S3. Geometries of each adsorption mode on stoichiometric mackinawite for model 1 (displaced H_2O on surface), 2 (displaced H_2O in the second coordination sphere) and 3 (displaced H_2O in the second coordination sphere with use of an implicit solvation model for water). Model 1 IS-mono-5 image previously used in SI of Ref. [17].

3 FeS-1O

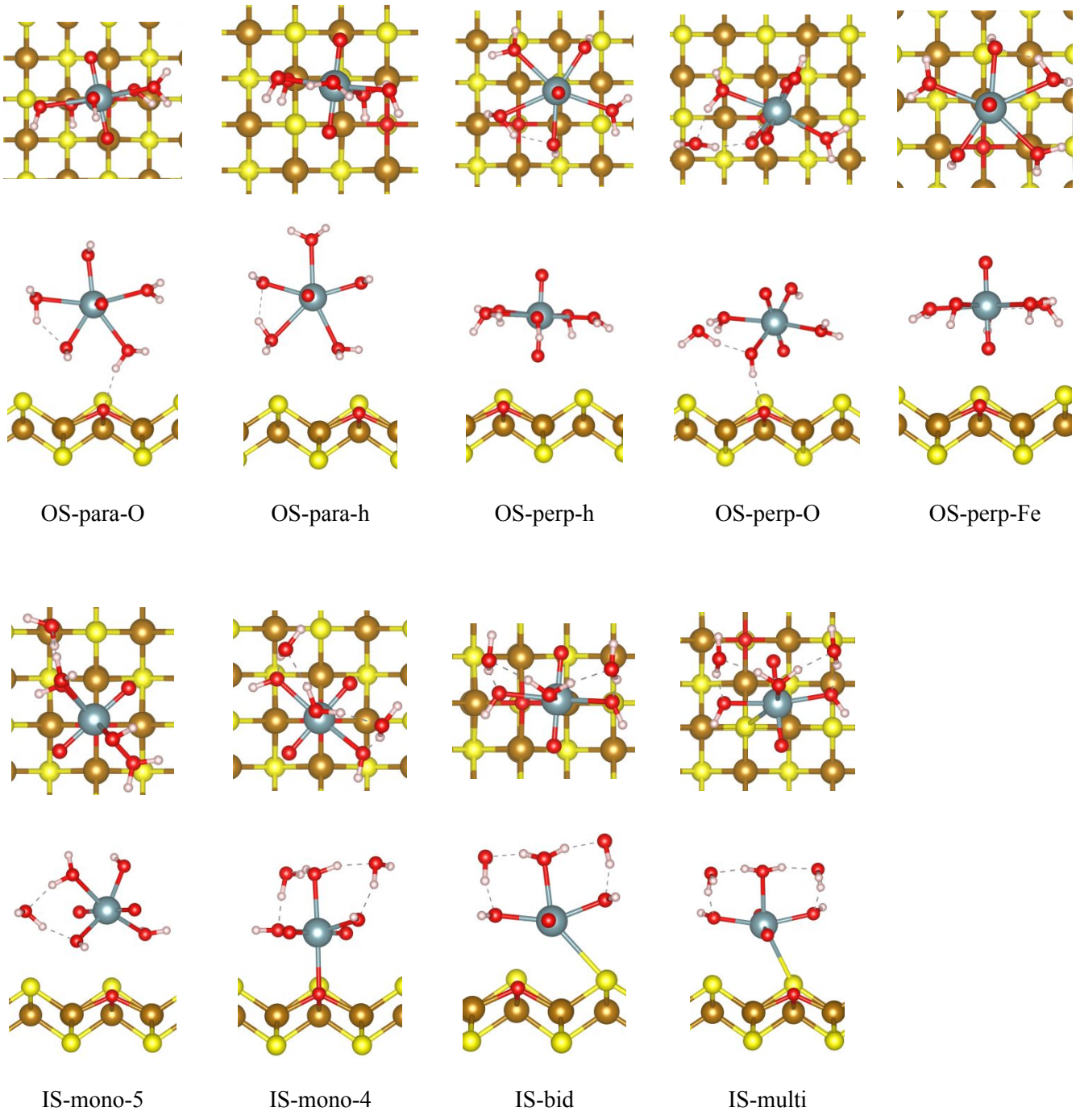

Figure S4. Top view and side view of each adsorption mode on FeS-1O.

Table S3. Adsorption energies, E_{ads}, U-O_{surf} distances and shortest U-S/Fe distances for all adsorption modes on the FeS-1O slab.

Adsorption mode	E_{ads} / kJ mol^{-1}	U-O_{surf} / Å	U-S / Å	U-Fe / Å
OS-para-O	-40	4.75	5.37, 5.59, 5.65, 5.92	5.70, 5.84, 5.85, 6.01
OS-para-h	-30	5.71	5.20, 5.40, 5.55	6.15, 6.17, 6.29, 6.32
OS-perp-h	-49	4.62	4.39, 4.55, 4.67	5.09, 5.16, 5.27, 5.34
OS-perp-O	-73	4.16	4.99, 5.35	5.14, 5.17, 5.38, 5.41
OS-perp-Fe	-47	4.46	4.32	4.99
IS-mono-5	-70	3.78	4.76, 4.86, 4.97, 5.07	4.82, 4.88, 4.94, 5.00
IS-mono-4	-65	2.56	4.14, 4.18, 4.26 ,4.30	3.84, 3.86, 3.90, 3.92
IS-bid	-42	2.97	3.17	3.59, 4.10, 4.21, 4.48, 4.58
IS-multi	-33	4.23	3.09, 3.60, 4.32	4.01, 4.18, 4.54, 4.67

4 FeS-2O

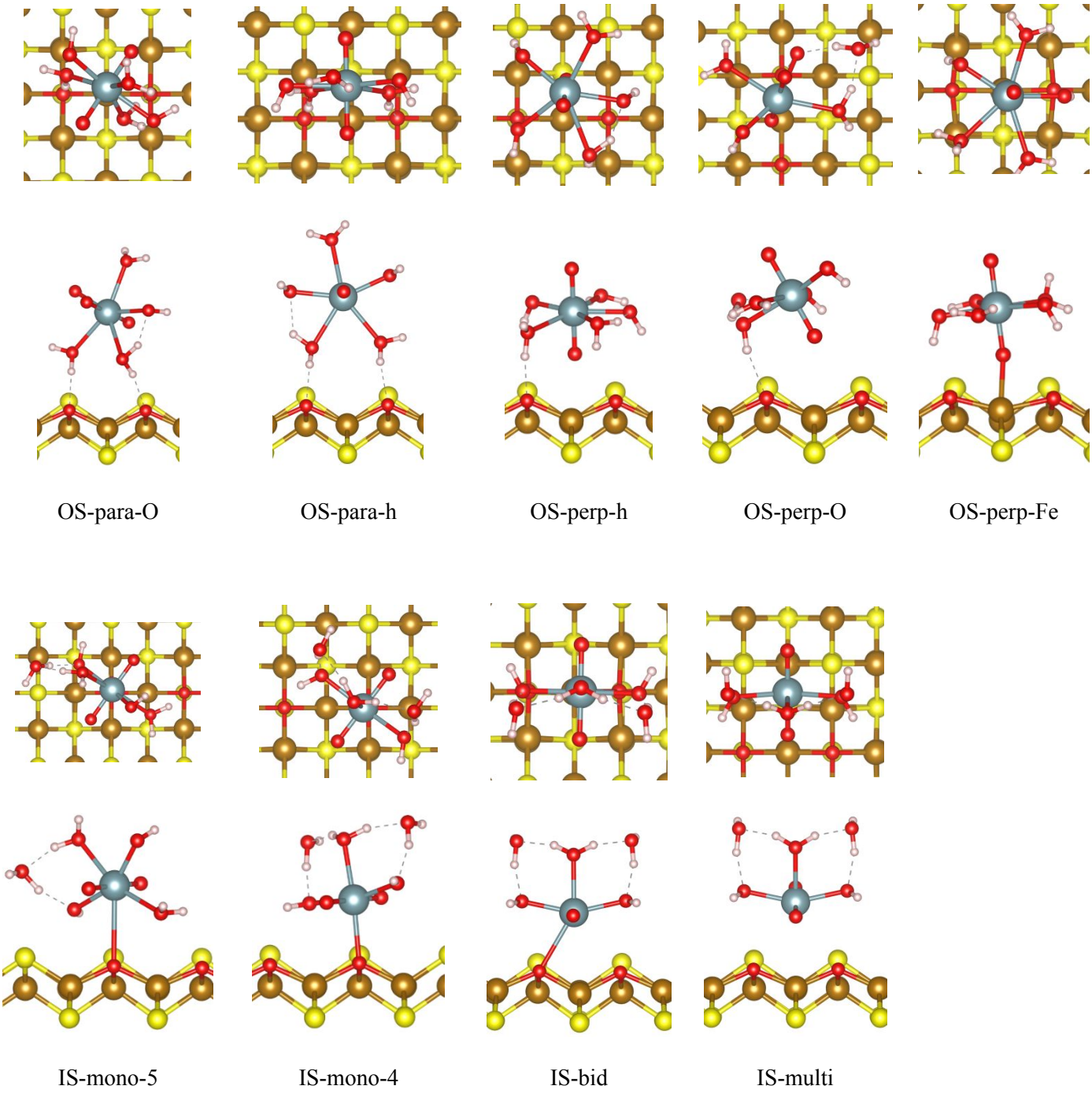

Figure S5. Top view and side view of each adsorption mode on FeS-2O.

Table S4. Adsorption energies, E_{ads}, U-O_{surf} distances and shortest U-S/Fe distances for all adsorption modes on the FeS-2O slab.

Adsorption mode	E_{ads} / kJ mol^{-1}	U-O_{surf} / Å	U-S / Å	U-Fe / Å
OS-para-O	-57	4.92, 4.93	5.45, 5.89, 5.90, 6.05, 6.08	5.45, 5.89, 5.90, 6.05, 6.08
OS-para-h	-47	5.14, 5.21	5.16, 5.26	5.68, 5.81, 5.89, 6.02
OS-perp-h	-61	4.18, 4.22	4.50, 4.55	4.55, 4.86, 4.91, 5.18
OS-perp-O	-80	4.04, 4.74	4.97, 5.18, 5.71	4.75, 5.08, 5.20, 5.46
OS-perp-Fe	-65	3.89, 4.11	4.81, 4.95, 5.14, 5.24	3.93, 4.82, 4.98, 4.99, 5.12
IS-mono-5	-77	3.27, 4.88	4.50, 4.66, 4.73	4.42, 4.46, 4.46, 4.54
IS-mono-4	-75	2.55, 4.25	4.21, 4.22, 4.39	3.77, 3.88, 3.88, 3.95
IS-bid	-46	2.88, 3.21	4.42, 4.46, 4.60, 4.61	3.45, 4.07, 4.09, 4.29, 4.30
IS-multi	-37	4.15, 4.16	3.25, 3.26	3.88, 4.16, 4.17, 4.36

References

1 P. E. Blöchl, Projector augmented-wave method, *Phys. Rev. B*, 1994, **50**, 17953–17979.

2 G. Kresse and D. Joubert, From ultrasoft pseudopotentials to the projector augmented-wave method, *Phys. Rev. B*, 1999, **59**, 1758–1775.

3 J. D. Pack and H. J. Monkhorst, 'special points for Brillouin-zone integrations'-a reply, *Phys. Rev. B*, 1977, **16**, 1748–1749.

4 J. P. Perdew, K. Burke and M. Ernzerhof, Generalized Gradient Approximation Made Simple, *Phys. Rev. Lett.*, 1996, **77**, 3865–3868.

5 J. P. Perdew, K. Burke and M. Ernzerhof, Generalized Gradient Approximation Made Simple-ERRATA, *Phys. Rev. Lett.*, 1997, **78**, 1396.

6 J. Chen and N. Kaltsoyannis, Computational Study of Plutonium−Americium Mixed Oxides (Pu0.92Am0.08O2−x); Water Adsorption on {111}, {110}, and {100} Surfaces, *J. Phys. Chem. C*, 2020, **124**, 6646–6658.

7 J. Chen and N. Kaltsoyannis, Computational Study of the Bulk and Surface Properties of Minor Actinide Dioxides MAnO2 (MAn = Np, Am, and Cm); Water Adsorption on Stoichiometric and Reduced {111}, {110}, and {100} Surfaces, *J. Phys. Chem. C*, 2019, **123**, 15540–15550.

8 B. E. Tegner and N. Kaltsoyannis, Multiple water layers on AnO2 {111}, {110}, and {100} surfaces (An = U, Pu): A computational study, *J. Vac. Sci. Technol. A*, 2018, **36**, 041402.

9 K. D. Kwon, K. Refson, S. Bone, R. Qiao, W. Yang, Z. Liu and G. Sposito, Magnetic ordering in tetragonal FeS: Evidence for strong itinerant spin fluctuations, *Phys. Rev. B*, 2011, **83**, 064402.

10 D. Welz and M. Rosenburg, Electronic band structure of tetrahedral iron sulphides, *J. Phys. C Solid State Phys.*, 2000, **20**, 3911–3924.

11 A. J. Devey, R. Grau-Crespo and N. H. De Leeuw, Combined density functional theory and interatomic potential study of the bulk and surface structures and properties of the iron sulfide mackinawite (FeS), *J. Phys. Chem. C*, 2008, **112**, 10960–10967.

12 S. Grimme, J. Antony, S. Ehrlich and H. Krieg, A consistent and accurate ab initio parametrization of density functional dispersion correction (DFT-D) for the 94 elements H-Pu, *J. Chem. Phys.*, , DOI:10.1063/1.3382344.

13 K. Mathew, R. Sundararaman, K. Letchworth-Weaver, T. A. Arias and R. G. Hennig, Implicit solvation model for density-functional study of nanocrystal surfaces and reaction pathways, *J. Chem. Phys.*, , DOI:10.1063/1.4865107.

14 K. Mathew and R. G. Hennig, Implicit self-consistent description of electrolyte in plane-wave density-functional theory, 2016, 1–6.

15 D. G. Archer and P. Wang, The Dielectric Constant of Water and Debye HÃ¼ckel Limiting Law Slopes, *J. Phys. Chem. Ref. Data*, 1990, **19**, 371–411.

16 A. R. Lennie, S. A. T. Redfern, P. F. Schofield and D. J. Vaughan, Synthesis and Rietveld Crystal Structure Refinement of Mackinawite, Tetragonal FeS, *Mineral. Mag.*, 1995, **59**, 677–683.

17 L. T. Townsend, S. Shaw, N. E. R. Ofili, N. Kaltsoyannis, A. S. Walton, J. F. W. Mosselmans,

T. S. Neill, J. R. Lloyd, S. Heath, R. Hibberd and K. Morris, Formation of a U(VI)-Persulfide Complex during Environmentally Relevant Sulfidation of Iron (Oxyhydr)oxides, *Environ. Sci. Technol.*, , DOI:10.1021/acs.est.9b03180.